CrossMark

ORIGINAL ARTICLE

Impacts of climate change on the hydro-climatology of the upper Ishikari river basin, Japan

Weili Duan[1,2] · Bin He[1] · Kaoru Takara[3] · Pingping Luo[3,4] · Daniel Nover[5] ·
Maochuan Hu[2]

Abstract Evidence for climate change impacts on the hydro-climatology of Japan is plentiful. The objective of the present study was to evaluate the impacts of possible future climate change scenarios on the hydro-climatology of the upper Ishikari River basin, Hokkaido, Japan. The Soil and Water Assessment Tool was set up, calibrated, and validated for the hydrological modeling of the study area. The Statistical DownScaling Model version 4.2 was used to downscale the large-scale Hadley Centre Climate Model 3 Global Circulation Model A2 and B2 scenarios data into finer scale resolution. After model calibration and testing of the downscaling procedure, the SDSM-downscaled climate outputs were used as an input to run the calibrated SWAT model for the three future periods: 2030s (2020–2039), 2060s (2050–2069), and 2090s (2080–2099). The period 1981–2000 was taken as the baseline period against which comparison was made. Results showed that the average annual maximum temperature might increase by 1.80 and 2.01, 3.41 and 3.12, and 5.69 and 3.76 °C, the average annual minimum temperature might increase by 1.41 and 1.49, 2.60 and 2.34, and 4.20 and 2.93 °C, and the average annual precipitation might decrease by 5.78 and 8.08, 10.18 and 12.89, and 17.92 and 11.23% in 2030s, 2060s, and 2090s for A2a and B2a emission scenarios, respectively. The annual mean streamflow may increase for the all three future periods except the 2090s under the A2a scenario. Among them, the largest increase is possibly observed in the 2030s for A2a scenario, up to approximately 7.56%. Uncertainties were found within the GCM, the downscaling method, and the hydrological model itself, which were probably enlarged because only one single GCM (HaDCM3) was used in this study.

✉ Weili Duan
duan.scut.cn@gmail.com

1 State Key Laboratory of Lake Science and Environment, Nanjing Institute of Geography and Limnology, Chinese Academy of Sciences, 73 East Beijing Road, Nanjing 210008, People's Republic of China

2 Department of Civil and Earth Resources Engineering, Graduate School of Engineering, Kyoto University, Kyoto, Japan

3 Disaster Prevention Research Institute, Kyoto University, Kyoto, Japan

4 School of Environmental Science and Engineering, Chang'an University, Xi'an 710064, China

5 Department of Engineering, University of California – Merced, 5200 North Lake Rd., Merced, CA 95343, USA

Introduction

The ongoing climate change has significantly affected the spatial and temporal distribution of water resources as well as the intensities and frequencies of extreme hydrological events (Coumou and Rahmstorf 2012). For example, distributions of precipitation in space and time are very uneven, leading to tremendous temporal variability in water resources worldwide (Oki and Kanae 2006). Increases in precipitation in the Northern Hemisphere midlatitudes, drying in the Northern Hemisphere subtropics and tropics, and moistening in the Southern Hemisphere subtropics and deep tropics were found (Zhang et al. 2007). The rate of evaporation, which depends on factors such as cloudiness, air temperature, and wind speed, varies a great deal, significantly affecting the amount of water

available to replenish groundwater supplies. The combination of shorter duration but more intense rainfall (meaning more runoff and less infiltration) combined with increased evapotranspiration (the sum of evaporation and plant transpiration from the earth's land surface to atmosphere) and increased irrigation is expected to lead to groundwater depletion (Konikow and Kendy 2005; Wada et al. 2010). It is therefore necessary to explore and understand the hydrological response of watersheds to climate change for improving the water resource planning and management.

In recent years, outputs (e.g., precipitation, temperature, humidity, and mean sea level pressure) at a global scale from general climate models (GCMs) are popularly downscaled to local-scale hydrological variables to compute and evaluate hydrological components for water resources variability and risk of hydrological extremes in the future (Taye et al. 2011; Tatsumi et al. 2013). Meenu et al. (2013) evaluated the impacts of possible future climate change scenarios on the hydrology of the catchment area of the Tungabhadra River, upstream of the Tungabhadra dam using the GCM HadCM3 outputs. Babel et al. (2013) characterized potential hydrological impact of future climate in the Bagmati River Basin, Nepal, and found annual basin precipitation will increase under both A2 and B2 scenarios. Based on outputs from six GCMs (CNRM-CM3, GFDL-CM2.1, INM-CM3.0, IPSL-CM4, MIROC3.2_M, and NCAR-PCM) under three emission scenarios (A1B, A2, and B1), Li et al. (2012) indicated extreme precipitation events will tend to occur in the southeast and northwest regions, while extreme temperature events happen in the north and southeast regions on the Loess Plateau of China during the twenty-first century.

Evidence for climate change impacts on the hydro-climatology of Japan is plentiful (Solomon 2007). The Japan Meteorological Agency (JMA) shows that annual average air temperatures nationwide rose by a rate equivalent to 1.15 °C per century between 1898 and 2010, which is considerably higher than the global average temperature rise of 0.74 °C over the last century (according to the Intergovernmental Panel on Climate Change's "Climate Change 2007: Synthesis Report Summary for Policymakers"); moreover, although no clear trends have been observed, the annual precipitation in Japan varies largely from year to year. All these changes in precipitation and temperature have greatly influenced water supply in Japan. For instance, concerning precipitation, years of low rainfall have become frequent since around 1970, and the amount of precipitation was much below average in 1973, 1978, 1984, 1994, and 1996, when water shortages caused damage. It tremendously affected drinking water supply because approximately 78% of it (actual record in the fiscal year 2004) is taken from rivers, lakes, marshes, and so forth. The possibility of frequent occurrence of extremely low rainfall, decrease in snowfall,

and earlier thaw will tend to increase the vulnerability of water resources. Meanwhile, extreme rainfall and temperature induced many hydrological disasters including floods, water quality incidents, and so on (Duan et al. 2015). Therefore, to predict and evaluate the temperature, precipitation, and surface water in japan is also necessary and important in the future.

Based on the GCMs output, lots of efforts at evaluation of hydro-climatology of Japan under climate change have been made. For example, Sato et al. (2013) investigated the impact of climate change on river discharge in several major river basins in Japan through a distributed hydrological simulation using the MRI-AGCM and found winter river discharge is projected to increase more than 200% in February, but decrease approximately 50–60% in May in the Tohoku and Hokuriku regions. In Agano River basin, the monthly mean discharge for the 2070s was projected to increase by approximately 43% in January and 55% in February, but to decrease by approximately 38% in April and 32% in May (Ma et al. 2010). However, there is less done on small river basins in Hokkaido about the hydro-climatology variations under climate change.

The objective of this study is to investigate the possible effects of climate change on water resources in the upper Ishikari River basin, Hokkaido, Japan, on the basis of outputs from GCM HadCM3. The paper is organized as follows: the study area, GCM output data, and methodology including SWAT model and downscaling techniques briefly described in the next section; the comparison results of temperature, precipitation, and waterflow in "Results" section, followed by discussions ("Discussion" section) and conclusions ("Conclusions and future work" section). The results of this study offer insights into hydrological response under climate change and provide tools for forecasting future climate conditions.

Study area, datasets, and methods

Study area

The upper Ishikari River basin (UIRB) is a headwater basin of the Ishikari River, which originates from Mt. Ishikaridake (elev. 1967 m) in the Taisetsu Mountains of central Hokkaido and flows southward into the broad Ishikari Plain and finally into the Sea of Japan, and is the third longest river in Japan (Fig. 1). The UIRB extends from the source of the Ishikari River in the Taisetsu Mountains and to an area of Asahikawa city. The geology of the UIRB is shown in Figure S1, suggesting there mainly has Jurassic-Cretaceous rocks, serpentinite and Cretaceous forearc sediment. This study focused on the watershed area above Ino discharge monitoring station (by the side of the Ishikari River, elev. 90.8 m), which is about 3, 450 km^2, approximately a quarter
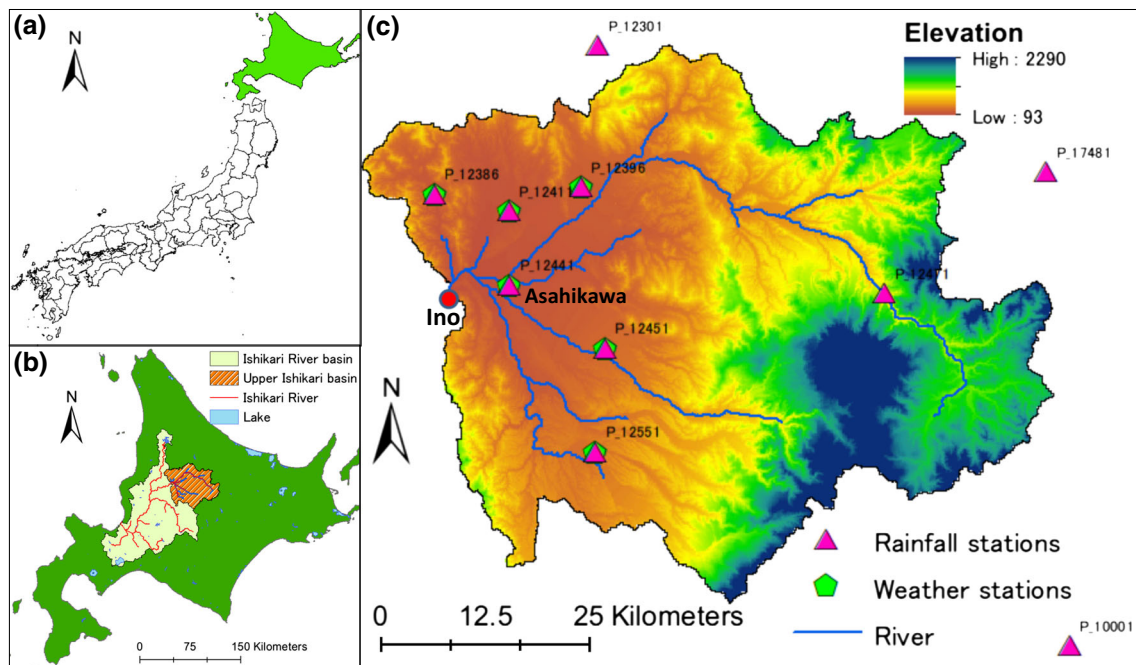
Fig. 1 Upper Ishikari River basin with stream gauge station (Ino station), rainfall stations and weather stations

of the Ishikari River basin, and the hydrograph of the Ishikari River from 1996 to 2005 is shown in Fig. 2. Runoff is mainly from snowmelt, especially from April to May. At the Asahikawa weather station (elev. 120 m) from 1981 to 2010, the mean annual, monthly air temperature in the warmest month (August) and the coldest month (January) are 6.9, 21.3 and −7.5 °C, respectively; the mean annual precipitation is 1042.00 mm. The UIRB area is covered in snow for as long as 5 months a year, from early December to late April.

SWAT model

The Soil and Water Assessment Tool (SWAT) model is a semi-distributed model that can be applied at the river basin scale to simulate the quality and quantity of surface and ground water and predict the environmental impact of land use, land management practices, and climate change (Arnold et al. 1998; Narsimlu et al. 2013). SWAT model uses hydrological response units (HRUs) to describe spatial heterogeneity in terms of land cover, soil type, and slope of land surface within a watershed. For each HRU, the model can estimate relevant hydrological components such as evapotranspiration, surface runoff, and peak rate of runoff, groundwater flow, and sediments yield. Currently, SWAT is embedded in an ArcGIS interface called ArcSWAT. The SWAT model simulates the hydrological cycle based on the water balance equation

$$SW_t = SW_0 + \sum_{i=1}^{t} (R_{day} - Q_{surf} - E_a - w_{seep} - Q_{gw}) \quad (1)$$

Fig. 2 Hydrograph of the Upper Ishikawa River (averages from 1996 to 2005)
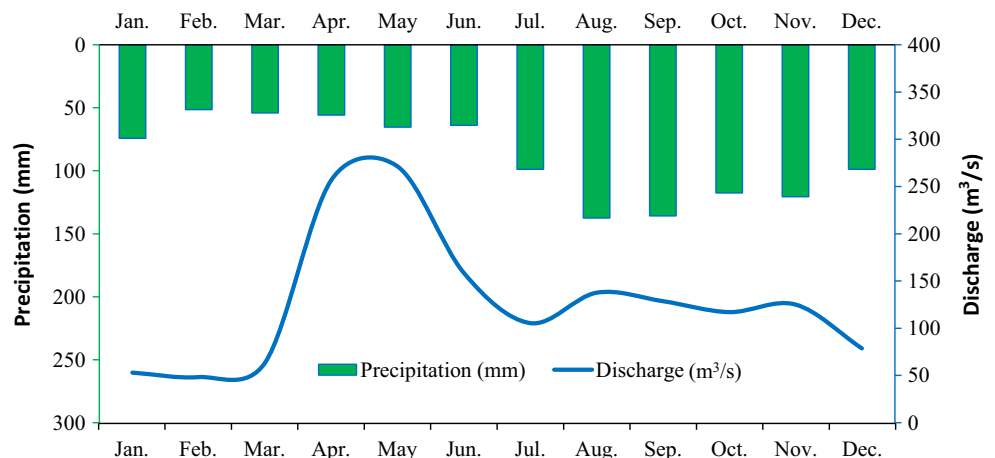
in which SW_t is the final soil water content (mm water), SW_0 is the initial soil water content in day i (mm water), t is the time (days), R_{day} is the amount of precipitation in day i (mm water), Q_{surf} is the amount of surface runoff in day i (mm water), E_a is the amount of evapotranspiration in day i (mm water), w_{seep} is the amount of water entering the vadose zone from the soil profile in day i (mm water), and Q_{gw} is the amount of return flow in day i (mm water). More detailed descriptions of the SWAT model principles are given by Neitsch et al. (2005).

SWAT model input datasets

Generally, the SWAT model requires the resolution digital elevation model (DEM) data, land use data, soil data, and climate data for calibrating the model. A 50-m grid resolution (DEM) data downloaded from National and Regional Policy Bureau, Japan, was used to delineate the UIRB and to analyze the drainage patterns of the land surface terrain in the ArcSWAT 2012 interface. The stream network characteristics such as channel slope, length, and width and the associated sub-basin parameters such as

slope gradient and slope length of the terrain were derived from the DEM. Land use is a very important factor that affects runoff, evapotranspiration, and surface erosion in a watershed. Soil type is one of the most important factors that significantly affect water transport in the soil because different soil types have different soil textural and physicochemical properties such as soil texture, available water content, hydraulic conductivity, bulk density, and organic carbon content. The land use and soil data were used for the definition of the HRUs. Land use data were developed using data derived from the Policy Bureau of the Ministry of Land, Infrastructure, Transport and Tourism, Japan, 2006, which mainly contains 11 types of land use. Here, the UIRB has nine types of land use (Fig. 3). Soil data were extracted from a 1:50,000 soil map of the Fundamental Land Classification Survey developed by the Hokkaido Regional Development Bureau (www.agri.hro. or.jp/chuo/kankyou/soilmap/html/map_index.htm). The daily weather data for precipitation, maximum and minimum temperature, wind speed, solar radiation, and relative humidity were obtained from the records of the rainfall and weather stations (Fig. 1) from 1981 to 2005. The daily river discharge data from 1995 to 2005 at the Inou station

Fig. 3 SWAT input datasets: slope (a), soil (b), and land use (c)
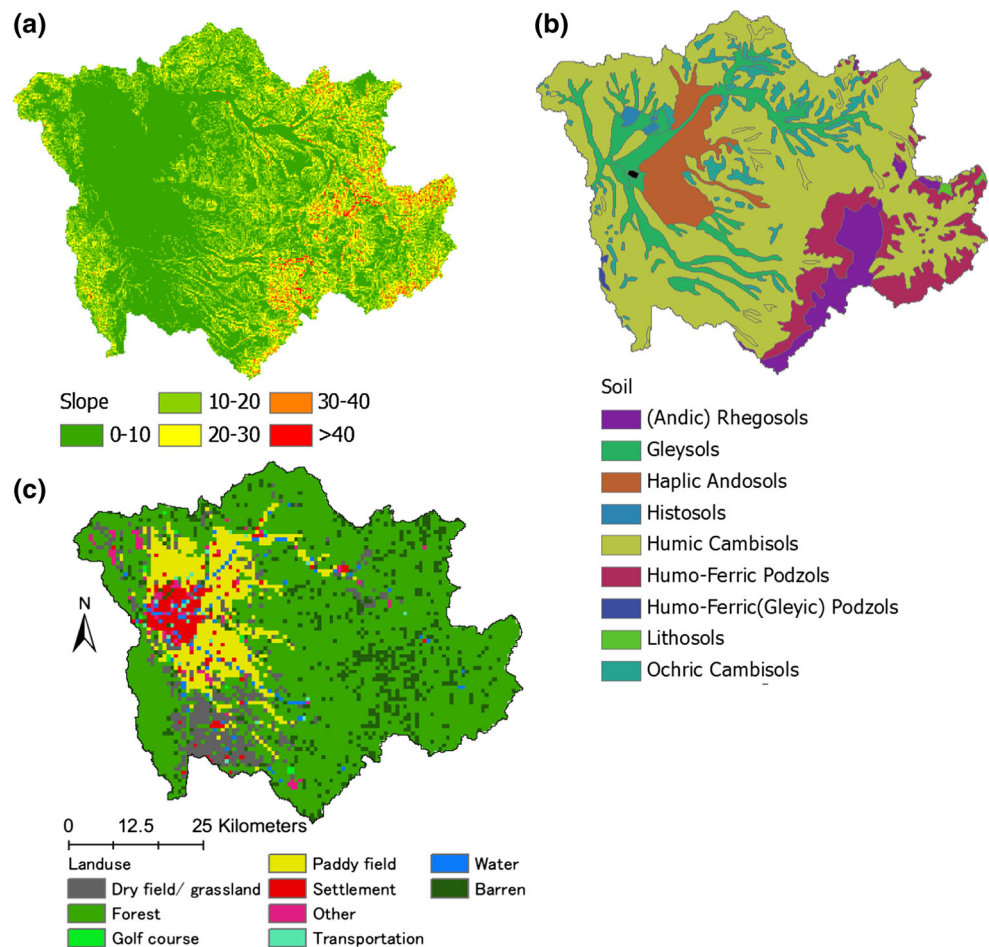
were downloaded from the Web site of the Japanese Ministry of Land, Infrastructure, and Transport (www1. river.go.jp), which were used for model calibration and validation.

Model setup and calibration

The model application involved six steps: (1) data preparation, (2) watershed and sub-basins discretization, (3) HRU definition, (4) parameter sensitivity analysis, (5) calibration and validation, and (6) uncertainty analysis. The steps for the delineation of watershed and sub-basins include DEM setup, stream definition, outlet and inlet definition, watershed outlets selection, and definition and calculation of sub-basin parameters. Here, the Ino river discharge monitoring station was chosen to be the outlet of the UIRB. Then, the resulting sub-basins were divided into HRUs based on the land use, soil, and slope combinations.

Sensitivity analysis was performed to delimit the number of parameters which affected the fit between simulated and observed data in the study area. The data for the period 1996–2000 were used for calibration, and data for the period 2001–2005 were used for validation of the model. Five years (1991–1995) were chosen as a warm-up period in which the model was allowed to initialize and then approach reasonable starting values for model state variables. The calibration and uncertainty analysis were done using the sequential uncertainty fitting algorithm (SUFI-2) in SWAT-CUP (Abbaspour et al. 2007).

To assess the performance of model calibration, the coefficient of the determination (R^2) and Nash–Sutcliffe efficiency (NSE) between the observations and the final best simulations are calculated. The former is usually used to evaluate how accurately the model tracks the variation of the observed values. The latter measures the goodness of fit and would approach unity if the simulation is satisfactorily representing the observed data, which describes the explained variance for the observed data over time that is accounted for by the SWAT model (Green and Van Griensven 2008). R^2 ranges between 0.0 and 1.0 and higher values mean better performance. NSE indicates how well the plot of observed values versus simulated values fits the 1:1 line and ranges from $-\infty$ to 1 (Nash and Sutcliffe 1970). Larger NSE values are equivalent with better model performance. Therefore, a few standards were adopted currently for evaluating model performance. For example, Santhi et al. (2001) used the standards of $R^2 > 0.6$ and NSE > 0.5 to determine how well the model performed. Chung et al. (2002) used the criteria of $R^2 > 0.5$ and NSE > 0.3 to determine if the model result is satisfactory. In this study, $R^2 > 0.5$ and NSE > 0.5 were chosen as criteria for acceptable SWAT simulation.

GCM data and NCEP predicators

GCMs are the most advanced tools and currently available for simulating the response of the global climate system to increasing greenhouse gas concentrations, which can provide global climatic variables under different emission scenarios. Because some researches (He et al. 2011; Tatsumi et al. 2014) indicated that the HadCM3 (Hadley Centre Coupled Model, version 3) GCM was chosen as representative for Japan area, the HadCM3 GCM output was considered suitable for the study watershed.

Large-scale predictor variables information including the National Centers for Environmental Prediction (NCEP_1961–2001) reanalysis data for the calibration and validation, and HadCM3 (Hadley Centre Coupled Model, version 3) GCM (H3A2a_1961–2099 and H3B2a_1961–2099) data for the baseline and climate scenario periods, was downloaded from the Canadian Climate Change Scenarios Network (http://www.cccsn.ec.gc.ca/). The NCEP reanalysis predictor contains 41 years of daily observed predictor data, derived from the NCEP reanalyzes, normalized over the complete 1961–1990 period. These data were interpolated to the same grid as HadCM3 (2.5 latitude × 3.75 longitude) before the normalization was implemented. The HadCM3 GCM predictor contains 139 years of daily GCM predictor data, derived from the HadCM3 A2 (a) and B2 (a) experiments, normalized over the 1961–1990 period. The predictors of the NCEP and HadCM3 GCM experiments with descriptions are presented in Table 1.

Downscaling techniques

Because the GCM output data are too coarse in resolution to apply directly for impact assessment in a certain area, it is necessary to downscale the GCM output data for bridging the spatial and temporal resolution gaps. Generally, downscaling techniques are divided into two main forms. One form is statistical downscaling, where a statistical relationship is established from observations between large-scale variables, like atmospheric surface pressure, and a local variable, like the wind speed at a particular site. Then, the relationship is subsequently used on the GCM data to obtain the local variables from the GCM output. The other form is dynamical downscaling, which can simulate local conditions in greater detail because the GCM output is used to drive a regional, numerical model in higher spatial resolution. Here, the statistical downscaling method was applied because of its simplicity and less computational time compared to dynamically downscaling (Wilby et al. 2000).

The statistical downscaling contains many methods such as regression methods, weather pattern-based approaches, stochastic weather generators. The Statistical DownScaling

Table 1 Daily predictor variable held in the grid box data archive

Variable	Description
temp	Mean temperature at 2 m
mslp	Mean sea level pressure
p500	500 hPa geopotential height
p850	850 hPa geopotentail height
rhum	Near surface relative humidity
r500	Reative humidity at 500 hPa height
r850	Relative humidity at 850 hPa height
shum	Near surface specific humidity
s500	Specific humidity at 500 hPa height
s850	Specific humidity at 850 hPa height

Derived variable: the following variables have been derived using the geostrophic approximation

**_f	Geostrophic air flow velocity
**_z	Vorticity
**_u	Zonal velocity component
**_v	Meridional velocity component
**zh	Divergence
**th	Wind direction

The derived variables have been derived using the geostrophic approximation

** Refers to different atmospheric levels: the surface (p_), 850 hPa height (p8), and 500 hPa height (p5)

Model (SDSM), which is a hybrid of a stochastic weather generator and a multivariate regression method for generating local meteorological variables at a location of interest (Wilby et al. 2002), was applied to assess the impacts of climate change under future climate scenarios in this study. Based on a combination of multi-linear regressions and a weather generator, the SDSM simulates daily climate data for current and future time periods by calculating the statistical relationships between predictand and predictor data series. As shown in Fig. 4, the procedures of the SDSM downscaling mainly contain six steps. The quality control was used to identify gross data errors and specify missing data codes and outliers prior to model calibration. The main purpose of the screen variable option is to choose the appropriate downscaling predictor variables. The calibrate model operation constructs downscaling models based on multiple regression equations, given daily weather data (the predictand) and regional-scale, atmospheric (predictor) variables. In this study, the ordinary least squares optimization was selected to evaluate the SDSM optimizes. The calibrated model was used to generate synthetic daily weather series using the observed (or NCEP reanalysis) atmospheric predictor variables and regression model weights. Then, the generated weather series was compared with observed station data to validate the model.

The SDSM bias correction was applied to compensate for any tendency to over- or underestimate the mean of conditional processes by the downscaling model (e.g., mean daily rainfall totals). The variance inflation scheme was also used to increase the variance of precipitation and temperatures to agree better with observations. When using bias correction and variance inflation, SDSM essentially becomes a weather generator, where a stochastic component is superimposed on top of the downscaled variable. This is especially true for precipitation, where the explained variance is generally less than 30% (Wilby et al. 1999).

Results

SWAT calibration and validation

In the discretization procedure, each available waterflow gauging station was imposed as a sub-basin outlet, and a threshold area of 10,000 ha (minimum area drained through a cell for the latter to be defined as a stream cell) was selected to discretize the watershed into sub-catchments of homogeneous size. In this study, the Inou station was the only waterflow gauging station that was used to calibrate the model. The UIRB was divided into 22 sub-basins with a total watershed area of 3,335 km^2, and the minimum, maximum, and mean elevation in the watershed were 91, 2290, and 608.2 m above mean sea level (amsl), respectively. The overlay of land use and soil grid maps resulted into 100 HRUs. The discretization was done trying to respect the original distribution of land use and soil, while keeping the number of HRUs down to a reasonable number.

Based on the sensitive SWAT-input parameters of Table 2, the SWAT model was calibrated on the observed monthly streamflow at the Inou gauging station. Figure 5 shows the simulated and observed monthly streamflows for both the calibration and validation periods. A more quantitative picture of the performance of the calibrated model for the calibration and validation period is gained from the two regression line plots of the simulated versus observed monthly streamflow of Fig. 6. For both periods, the regression lines have a slope close to 1, indicting a good agreement between the monthly observed and simulated streamflows. The values of the statistical parameters NSE for both the calibration and validation periods were 0.87 and 0.86, respectively, exhibiting that calibration results were in a reasonable agreement between monthly observed and simulated streamflows.

From the calibration and validation results, it may be deduced that the model represents the hydrological

Fig. 4 SDSM downscaling procedures (modified from Wilby and Dawson 2007)
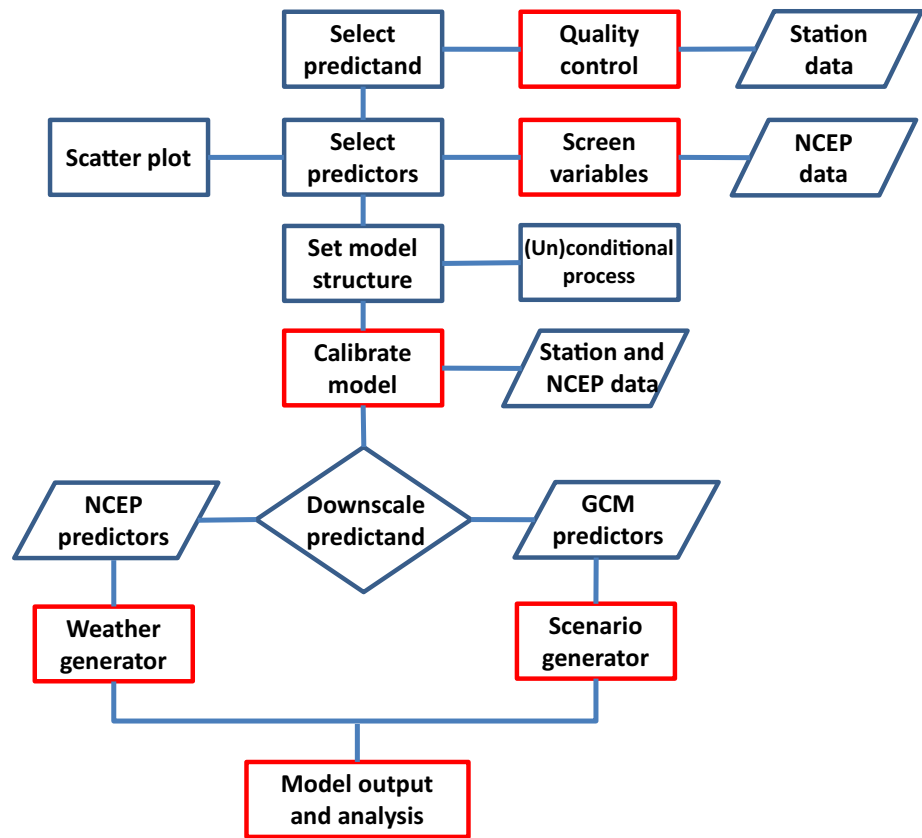

Table 2 Parameter global sensitivity ranking and final auto-calibration results

Rank	Parameter	Description	Optimal value	Lower bound	Upper bound
1	SFTMP	Snowfall temperature (°C)	4.358	−5	5
2	ESCO	Soil evaporation compensation factor	0.307	0	1
3	GW_REVAP	Groundwater "revap" coefficient	0.694	0	1
4	SOL_K	Saturated hydraulic conductivity	−0.666	−0.8	0.8
5	SOL_AWC	Available water capacity of the soil layer (mm H_2O mm^{-1} soil)	0.184	−0.5	1
6	GWQMN	Shallow aquifer required for the return flow to occur (mm)	0.112	0	2
7	GW_DELAY	Groundwater delay (days)	68.25	0	1000
8	ALPHA_BF	Baseflow alpha factor (days)	0.059	0	1
9	CH_N2	Manning's "n" value for the tributary channels	0.164	0	0.3
10	SMFMN	Minimum melt rate for snow during years (mm $°C^{-1}day^{-1}$)	4.03	0	8
11	SMFMX	Maximum melt rate for snow during years (mm $°C^{-1}day^{-1}$)	4.402	0	8
12	CN2	Initial SCS runoff curve number for moisture condition II	−0.163	−0.2	0.8

characteristics of the watershed and can be used for further analysis.

Climate projects

SDSM validation

Changes in precipitation, maximum temperature and minimum temperature at the Asahikawa station were downscaled using the SDSM 4.2. The Asahikawa station can be taken to be representative of all stations in the UIRB area since the UIRB area is relatively small compared to the GCM's resolution. The calibration was carried out from 1961 to 1981 for 21 years, and the withheld data from 1982 to 2001 were used to validate the model. Figures 7, 8, 9 and 10 show the performance of the simulated versus observed daily maximum temperature, minimum temperature, and precipitation during calibration and validation periods, respectively,
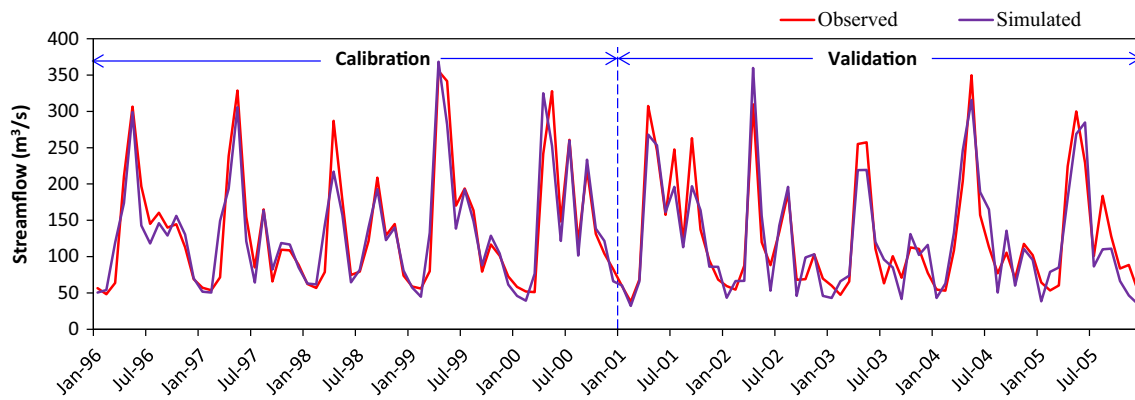
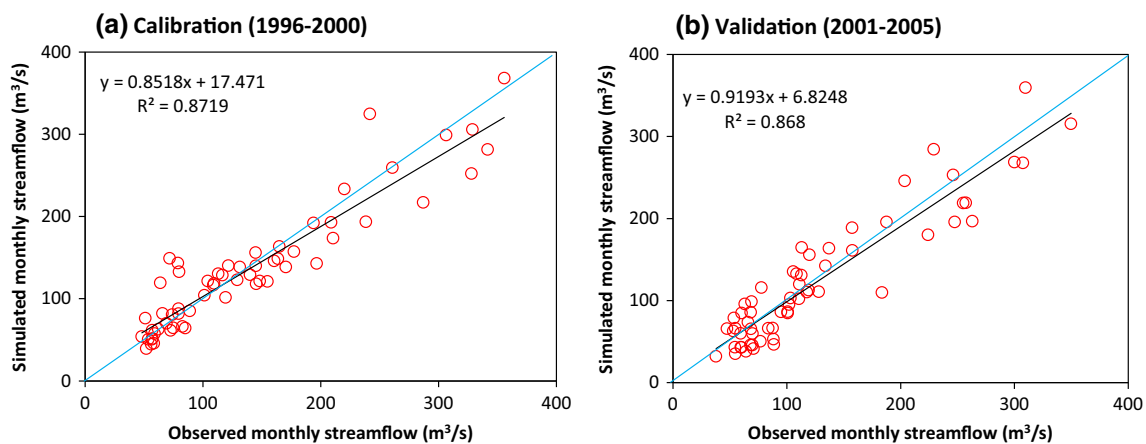**Fig. 5** Simulated and observed monthly streamflow for calibration- and validation periods

Fig. 6 Scatter-plot of simulated versus observed monthly streamflow during calibration (**a**) and validation (**b**)

which indicate good agreement between the simulated and observed values of daily maximum and minimum temperature, but bad in daily precipitation. Maybe it is because rainfall predictions have a larger degree of uncertainty than those for temperature since precipitation is highly variable in space and the relatively coarse GCM models cannot adequately capture this variability (Wilby and Dawson 2007; Bader et al. 2008). As shown in Figs. 10 and 11, however, the comparison between observed average long-term mean monthly precipitation, and maximum and minimum temperature with corresponding simulations indicated that the results of the SDSM generally replicated the basic pattern of observations.

The climate scenario for the future periods in the UIRB area was developed from statistical downscaling using the HadCM GCM predictor variables for the two Emissions Scenarios (SRES) including A2a and B2a based on the 20 ensembles, and the analysis was done based on 20-year periods centered on the 2030s (2020–2039), 2060s (2050–2069), and 2090s (2080–2099). A2a describes a highly heterogeneous future world with regionally oriented economies, the main driving forces of which are a high rate

of population growth, increased energy use, land use changes, and slow technological change. The B2a is also regionally oriented but with a general evolution toward environmental protection and social equity.

Future temperature

As shown in Figs. 12 and 13, the mean monthly, seasonal, and annual changes in daily temperature from the baseline period data exhibited an increasing trend for both scenarios (A2a and B2a) in 2030s, 2060s, and 2090s, and increases in the A2a scenario are much bigger than in the B2a scenario.

The average annual maximum temperature might increase by 1.80 and 2.01, 3.41 and 3.12, and 5.69 and 3.76 °C in 2030s, 2060s, and 2090s for A2a and B2a emission scenarios, respectively. Results from the seasonal scale reveal that summer has the highest increases under both A2a and B2a emission scenarios in 2090s, up to 6.27 and 3.96 °C, respectively, while autumn has the lowest increases with approximately 5.24 and 3.59 °C, respectively. Monthly, the largest increase in mean maximum temperature is indicated during the August for both A2a
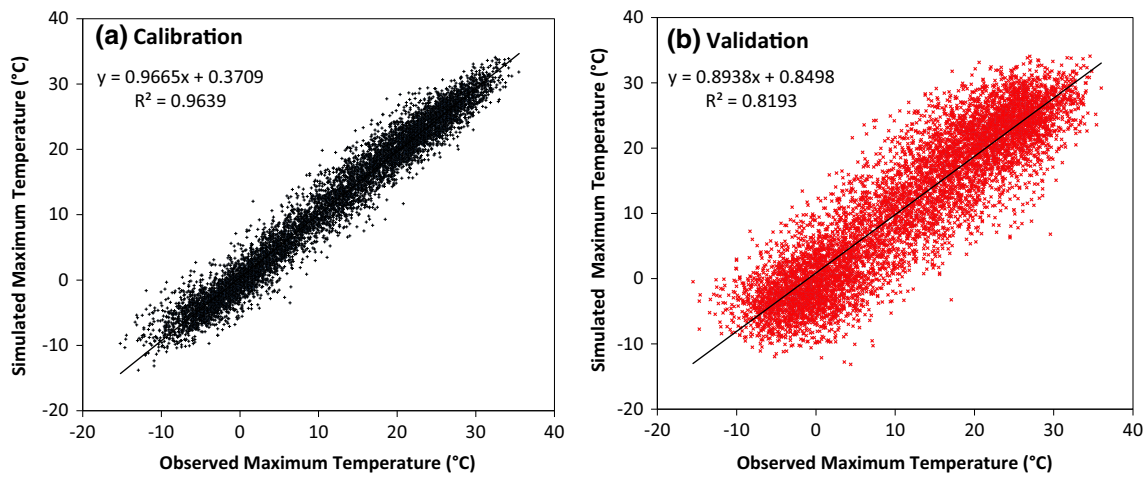
Fig. 7 Scatter plot of simulated versus observed daily maximum temperature during calibration (**a**) and validation (**b**)
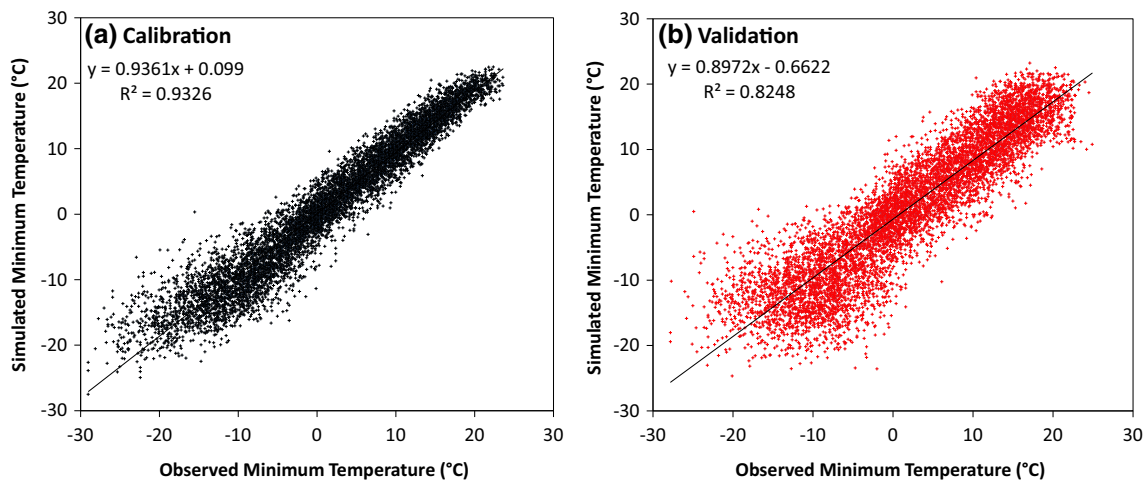

Fig. 8 Scatter plot of simulated versus observed daily minimum temperature during calibration (**a**) and validation (**b**)
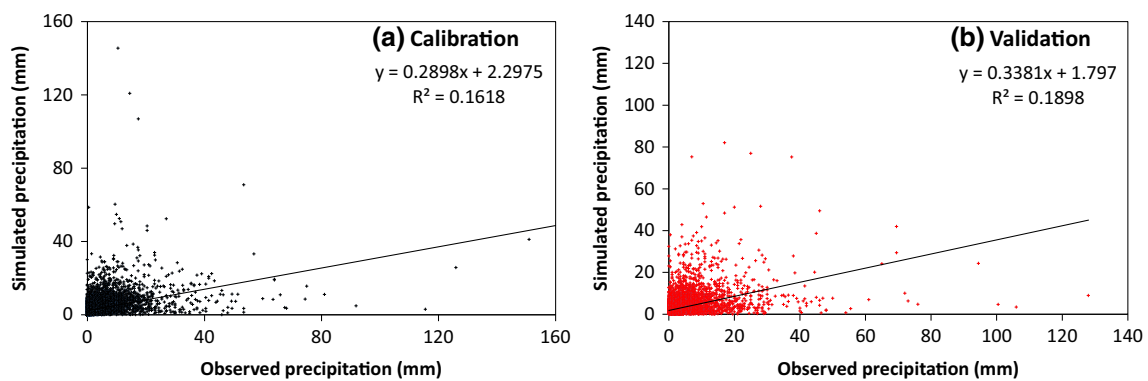

Fig. 9 Scatter plot of simulated versus observed daily precipitation during calibration (**a**) and validation (**b**)

(approximately 7.40 °C) and B2a (approximately 4.59 °C) emission scenarios in 2090s.

Results for minimum temperature indicated that the average annual minimum temperature might increase by 1.41 and 1.49, 2.60 and 2.34, and 4.20 °C and 2.93 in 2030s, 2060s, and 2090s for the A2a and B2a emission scenarios, respectively. Seasonally, winter has the largest increase for both scenarios in each period, followed by
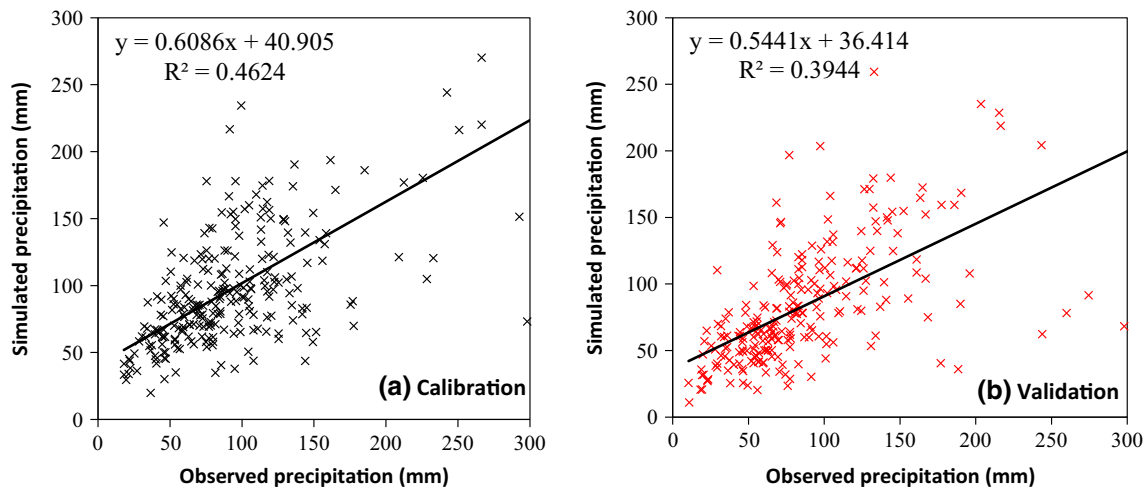
Fig. 10 Scatter plot of simulated versus observed monthly precipitation during calibration (**a**) and validation (**b**)
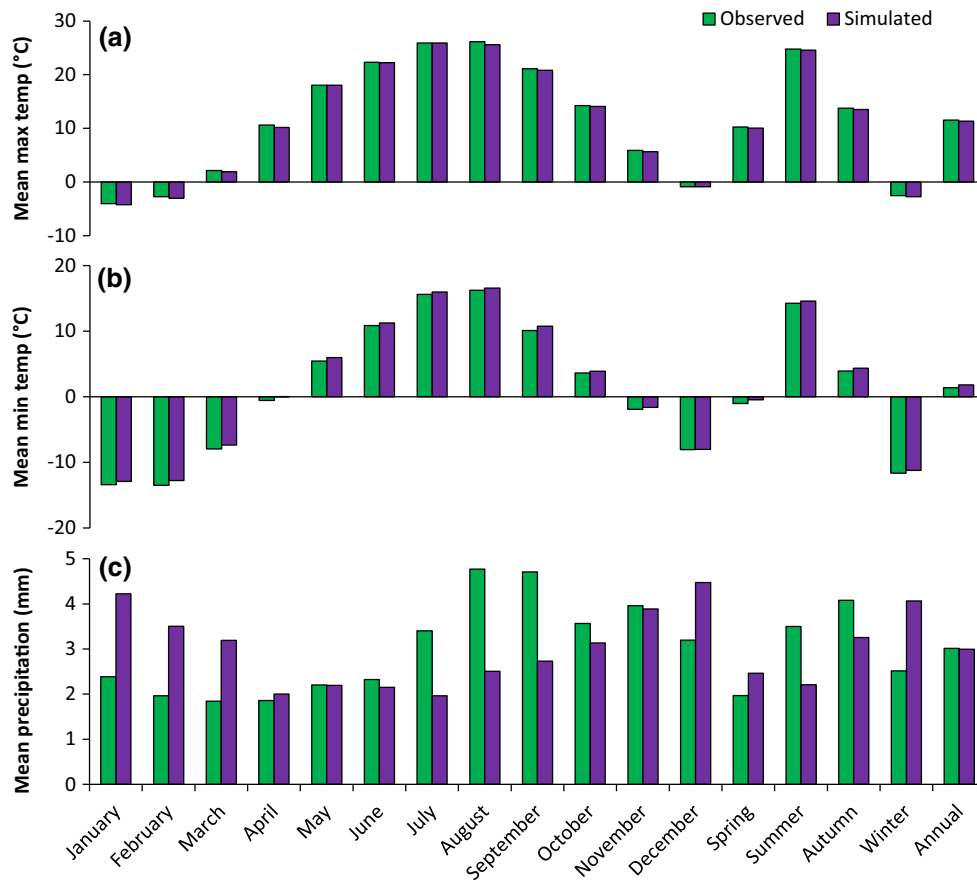

Fig. 11 Comparison between observed and generated mean daily precipitation and maximum and minimum temperature values in the time step for the Inou station. **a** Maximum temperature (°C), **b** minimum temperature (°C), and **c** precipitation (mm)

summer, autumn, and spring. For the 2090s, the average minimum temperature in winter possibly increases by 5.17 and 2.66 °C for A2a and B2a scenarios, respectively. As in the case of monthly simulation, the minimum temperature tends to increase during all twelve months for

both scenarios in all future periods (Fig. 13). August has the largest increase (around 6.74 °C) under the A2a scenario in 2090s, followed by January (around 6.05 °C) and July (around 5.73 °C); January has the largest increase (around 4.40 °C) under the B2a scenario in 2090s,
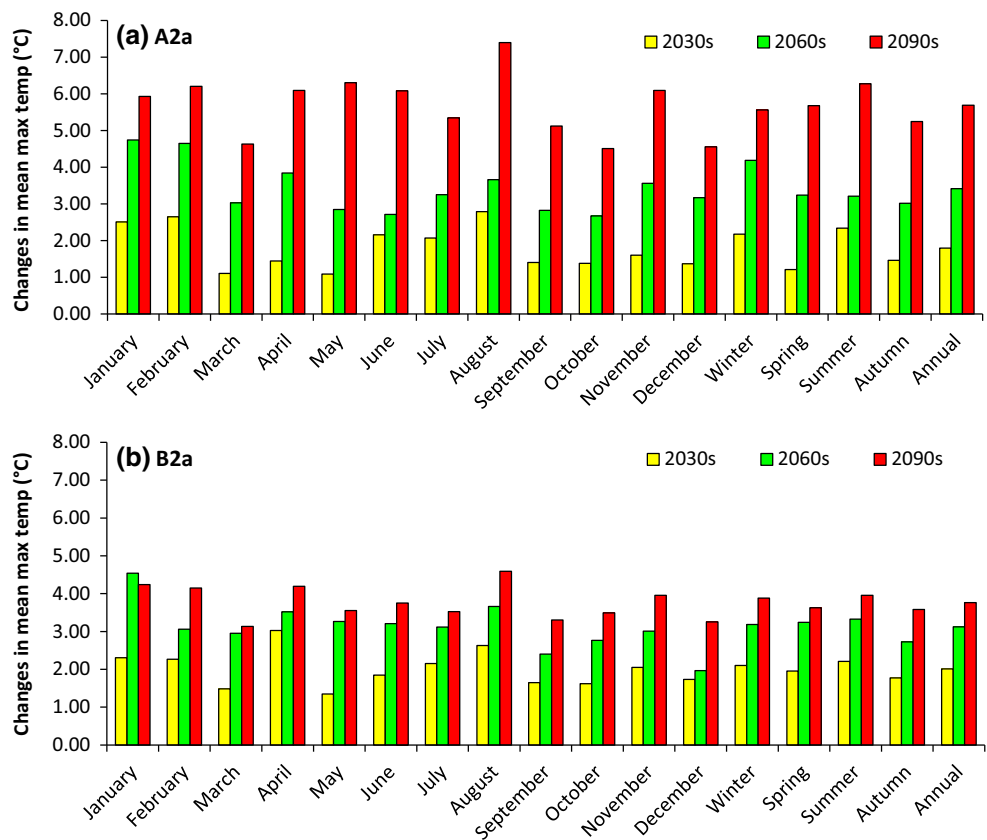
followed by August (around 4.24 °C) and July (around 3.82 °C).

Future precipitation

Figure 14 shows that the average annual precipitation might decrease by 5.78 and 8.08, 10.18 and 12.89, and 17.92 and 11.23% in the future 2030s, 2060s, and 2090s for A2a and B2a emission scenarios, respectively, suggesting that a remarkable decreasing trend in precipitation is likely to appear in the UIRB area in the future. On a seasonal timescale, there may be a decrease in mean precipitation for all seasons under both scenarios except for winter in 2030s and 2060s and spring in 2030s under A2a scenario. Among them, autumn has the largest decrease, up to 9.52, 20.12, and 25.22 for the 2030s, 2060s, and 2090s, respectively, for A2a scenario, and 12.49, 14.66, and 20.49% for B2a scenario, followed by summer, spring, and winter. Simulation results for the average monthly precipitation indicate that there is a mixed trend. As shown in Fig. 13, in the 2030s there may be a decrease in mean monthly precipitation for all months except for February, April, May, and December under A2a scenario, and February and May under B2a scenario. In addition, there may be an increasing trend in both February and December for all three future periods for A2a scenario as compared to the base period.

More decreases are observed in September for the 2090s for both A2a (approximately 35.47%) and B2a (approximately 27.05%) scenarios compared to other months, and the largest decrease is also found in September for the 2060s for the A2a scenario, up to 38.90%.

Climate change impact

The impact of climate change on waterflow was predicted and analyzed taking the waterflow from 1981 to 2000 as the baseline flow against which the future flows for the 2030s, 2060s, and 2090s compared. Precipitation and maximum and minimum temperatures are the climate change drivers, which were inputted into the calibrated SWAT model to fulfill the climate impact assessment. Figure 15 shows the percentage changes in mean monthly, seasonal, and annual flow volume for the future 2030s, 2060s, and 2090s periods compared to the baseline period (1981–2000) at the Inou gauging station, suggesting that there may be the same trend in A2a and B2a emission scenarios.

Results indicate an increase in annual mean streamflow for the all three future periods except the 2090s under the A2a scenario. Among them, the largest increase is observed in the 2030s for A2a scenario, up to approximately 7.56%.
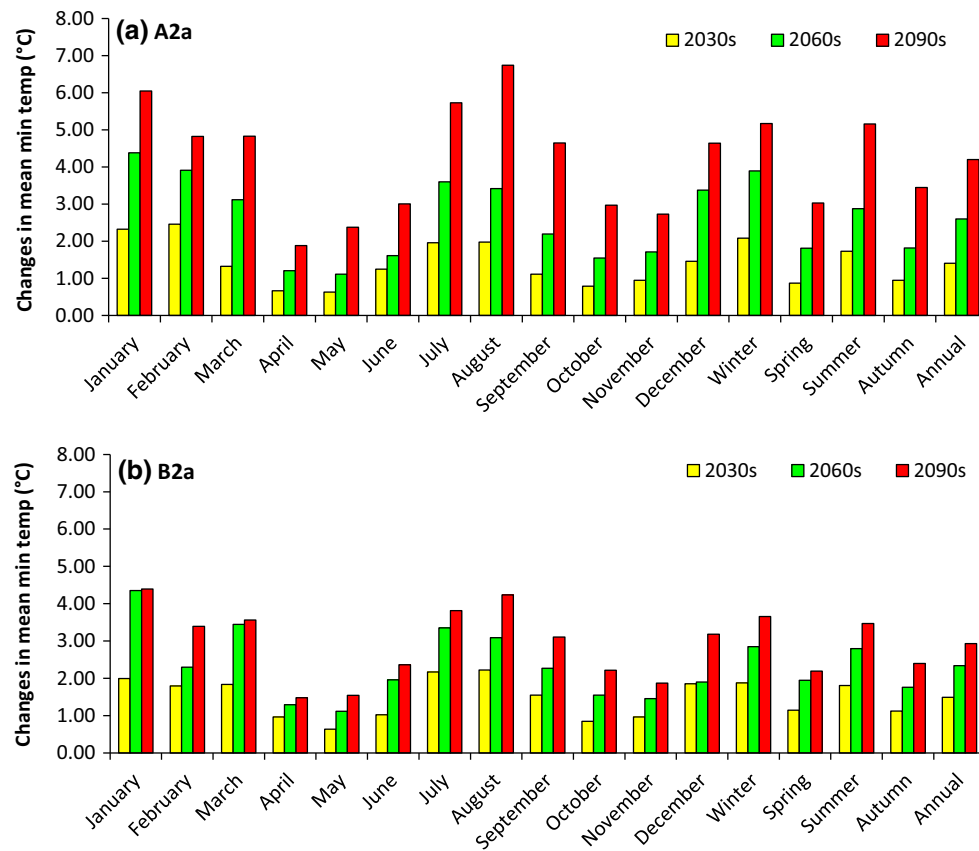
Fig. 13 Changes in monthly, seasonal, and annual mean minimum temperature for the future 2030s, 2060s, and 2090s periods as compared to the baseline period (1981–2000) at Inou station. **a** A2a scenario and **b** B2a scenario

As in the case of seasonal prediction, a pronounced increase is exhibited in winter for the all future periods for both scenarios, while a decrease is found in summer except the 2030s for A2a scenario. The highest increase is up to 72.17% in the 2060s under A2a scenario, followed by 70.89% in the 2090s under A2a scenario and 62.61% in the 2090s under B2a scenario, and the largest decrease is about 22.09%, which is predicted in the 2090s under A2a scenario. Spring and autumn have a mixed and slight trend for future periods for both scenarios.

On a monthly scale, an increasing trend is found in January, February, March, July, and December for all future periods for both scenarios, while a decrease may happen in April and June. For the 2030s, the mean monthly flow shows an increase for all months except April and June in both scenarios. In this period, the highest increase is up to 135.86% for the B2a scenario, followed by 110.19 and 81.99% for the A2a scenario; on the other hand, the largest decrease is up to 40.07% for the B2a scenario, followed by 32.46% for the A2a scenario and 19.21% for the B2a scenario. There are more months in which mean precipitation is likely to decrease in the 2060s and 2090s compared to the 2030s.

Discussion

Using the outputs from HadCM3 GCM A2a and B2a climatic scenarios, the changes in temperature, precipitation, and the waterflow were evaluated on the Upper Ishikari River Basin for the 2030s, 2060s, and 2090s periods. The SDSM statistical downscaling tool was applied to compute the future temperature and precipitation. All these data were inputted into the calibrated SWAT model for calculating the waterflow for all three periods under both scenarios. All the results obtained from this study are representative for a majority of GCM output, and therefore our results are plausible estimates of future effects of climate change in the UIRB area. These findings also generate several interesting questions despite clearly indicating significant changes in hydro-climatology in the UIRB area in the future.

First, performance of the downscaling results in daily maximum temperature and minimum temperature is very good, but relatively bad in daily precipitation. Some other researches got the similar results in the downscaled daily precipitation (Dile et al. 2013). Bader et al. (2008) pointed out the prediction of rainfall by GCMs is often poor as the
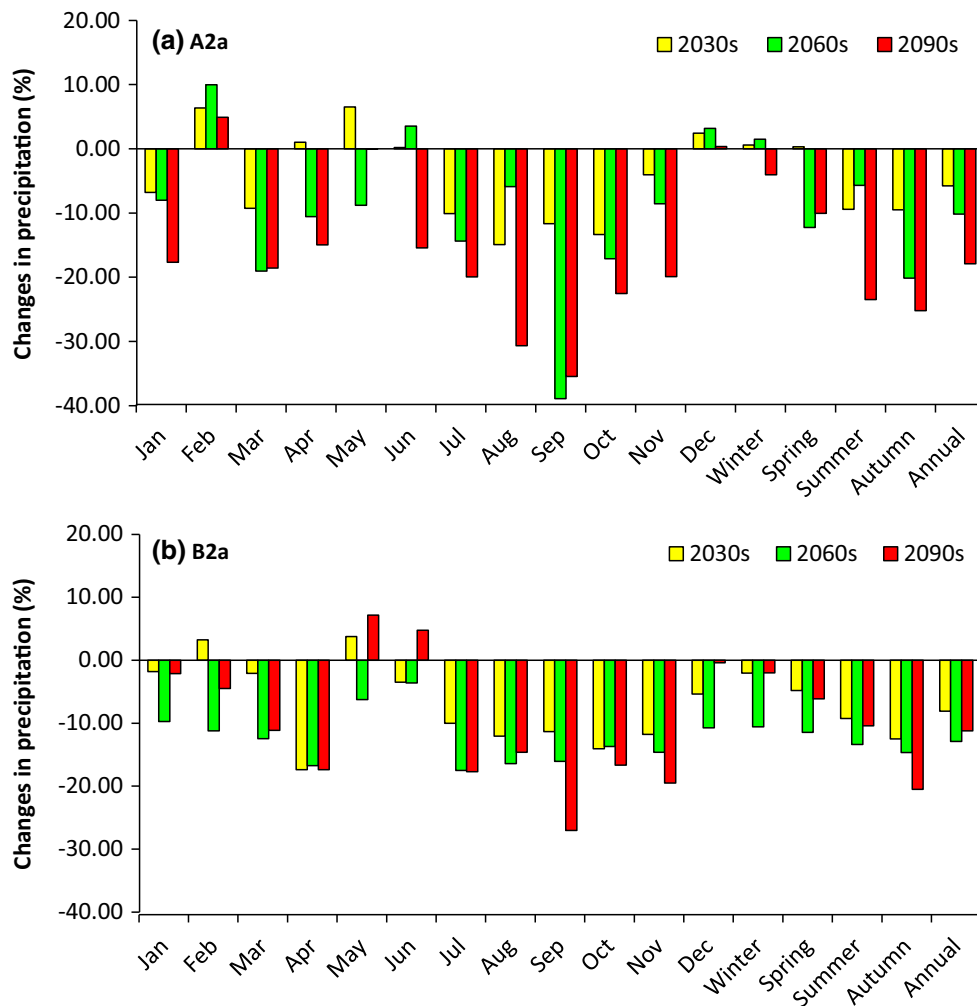
Fig. 14 Changes in monthly, seasonal, and annual mean precipitation values for the future 2030s, 2060s, and 2090s periods as compared to the baseline period (1981–2000) at Inou station. **a** A2a scenario and **b** B2a scenario

variables that force rainfall patterns are dominated by topography and to a lesser extent vegetation. Prudhomme et al. (2002) also indicated that the current generation of GCMs still does not provide reliable estimates of rainfall variance, and it is currently difficult to develop appropriate downscaling methodologies. For example, the rainfall patterns predicted by ensembles of GCMs for India completely miss the higher rainfall areas of the sub-Himalaya and the Western Ghats, although they slightly overestimate the current average rainfall, while modeled peak daily rainfall intensity was only two-thirds of that recorded. All these may be the reasons for getting the relative bad performance for the daily precipitation prediction.

In addition, the annual precipitation exhibits a decreasing trend in the future, but the waterflow shows no trends or even increasing trend. Also, this situation appears in the some months (e.g., January, March). The waterflow is expected to change according to temperature and precipitation changes. Obviously, remarkable decreasing trend

(i.e., the average annual precipitation may decrease by 5.78% and 8.08, 10.18 and 12.89%, and 17.92 and 11.23% in the future 2030s, 2060s, and 2090 for A2a and B2a emission scenarios, respectively) in precipitation will be likely to reduce the runoff in the UIRB area. Temperature, however, will tend to increase, which contributes to the snow melting. The UIRB area is located in Hokkaido, which is covered in snow for as long as 4 months a year. From the results of calibrated SWAT model, the temperature was sensitive to streamflow in the UIRB area; that is, snowfall temperature (STFMP), minimum melt rate for snow during years (SMFMN), and maximum melt rate for snow during years (SMFMX) will significantly affect the river flow. The average annual maximum temperature possibly increases by 1.80 and 2.01, 3.41 and 3.12, and 5.69 and 3.76 °C in 2030s, 2060s, and 2090s for A2a and B2a emission scenarios, respectively, which will extremely increase snowmelt. As a result, the annual mean streamflow will be likely to increase for the all three future
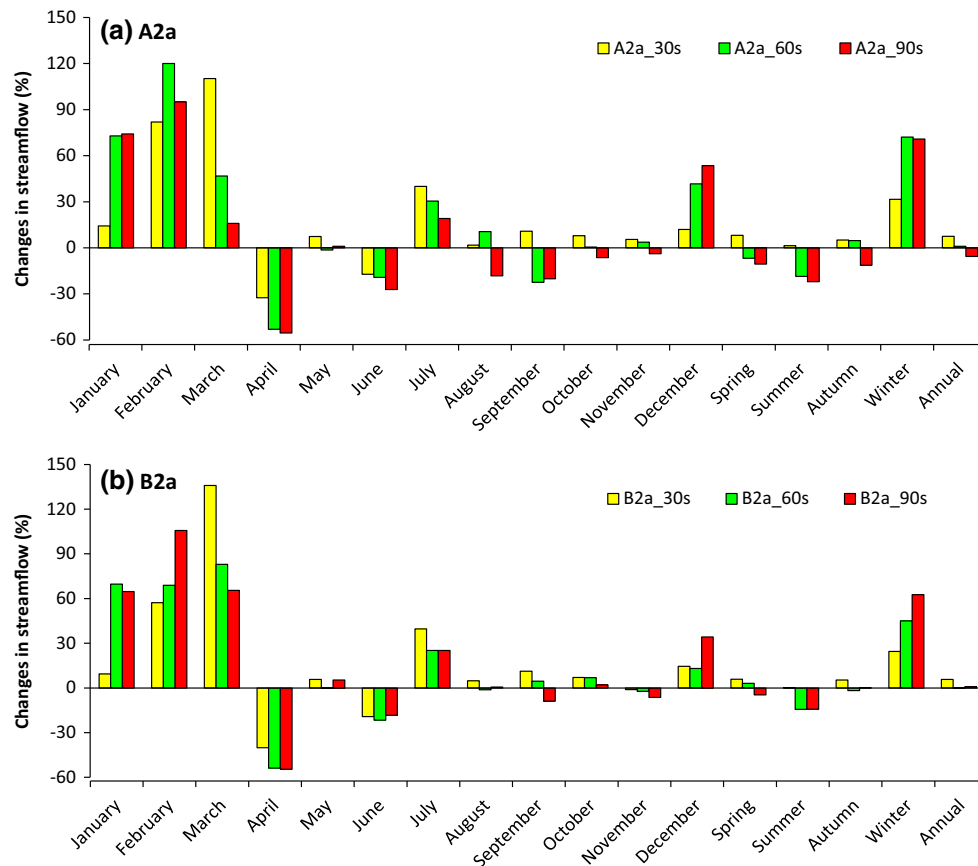
Fig. 15 Percentage change in mean monthly, seasonal, and annual flow volumes for the future 2030s, 2060s, and 2090s periods as compared to the baseline period (1981–2000) at the Inou gauging station. **a** A2a scenario and **b** B2a scenario

periods except the 2090s under the A2a scenario, and the largest increase will be observed in the 2030s for A2a scenario, up to approximately 7.56%. These variations are also in line with the results of (Sato et al. 2013). Considering these impacts, it is worth emphasizing the importance of mitigation and adaptation to climate change and we suggest the following actions: (1) Identify relevant risk and vulnerable to weather-related events and snowmelt hazards; (2) change national standards, such as building stream channels, levees, and dams, to address increase in stream flow; and (3) develop community by-laws to regulate building construction to minimize pressure on flooding.

Finally, although the results from the cascade of models in this study indicated a satisfactory and acceptable performance, there is much uncertainty in all used models. It is a combination of uncertainties in catchment discretization in SWAT model, the hydrological parameter university (Maurer and Duffy 2005), GCM outputs as a result of the downscaling (Chen et al. 2011), and neglect of land use changes or potential changes in soil properties (Setegn et al. 2011). As shown in Table 2, not all the SWAT parameters were discussed except for some main parameters that greatly affect the water balance, and therefore it is

not sufficient to elaborate hydrological changes because of the snow to rainfall shift in precipitation regime and the associated seasonal shift (earlier snowmelt and/or more summer drought). Only 22 sub-basins and 100 HRUs were divided for the whole basin, which may weaken the impacts on water cycle from topographical and land use variability. It is also extremely risky to calibrate a catchment that as large as the Upper Ishikari (>3000 km^2) with only one single gauging station in this study, which cannot perfectly simulate the water resource balance. Moreover, HaDCM3 GCM outputs have kind of uncertainty, which cannot perfectly simulate the future (Buytaert et al. 2009). So, each GCM output will give different results. In this study, we focused on the UIRB area by downscaling HaDCM3 outputs, and there are probably some different results if some other GCMs would be used. Downscaling techniques also bring some uncertainties (Khan et al. 2006; Fowler et al. 2007). For example, Prudhomme and Davies (2009) found some times bias is not visible with SDSM-downscaled scenarios although there is a tendency toward underestimation, but this is within natural variability. Thirdly, we neglected land use changes or potential changes in soil properties; however, land cover will change due

to natural and anthropogenic influences and corresponding features should be changed in the model.

Conclusions and future work

SWAT model was successfully applied to simulate the possible effects of climate change on water resources in the UIRB on the basis of projected climate conditions by using GCM out puts of HadCM3 SRES A2a and B2a emissions scenarios with Statistical Downscaling (SDSM) modeling approach. Major conclusions can be summarized as follows: (1) The values of the statistical parameters NSE for both the calibration and validation periods were 0.87 and 0.86, respectively, exhibiting calibration results were in a reasonable agreement between monthly observed and simulated streamflows, and therefore it could be used to evaluate the hydrological response under the climate change in the UIRB area; (2) the downscaling results indicated that the average annual maximum temperature might increase by 1.80 and 2.01, 3.41 and 3.12, and 5.69 and 3.76 °C, the average annual minimum temperature might increase by 1.41 and 1.49, 2.60 and 2.34, and 4.20 and 2.93 °C, and the average annual precipitation might possibly decrease by 5.78 and 8.08, 10.18 and 12.89, and 17.92 and 11.23% in 2030s, 2060s and 2090s for A2a and B2a emission scenarios, respectively; (3) the annual mean streamflow will be likely to increase for the all three future periods except the 2090s under the A2a scenario. Among them, the largest increase is observed in the 2030s for A2a scenario, up to approximately 7.56%. Also, a pronounced increase is exhibited in winter for the all future periods for both scenarios, while a decrease is found in summer except the 2030s for A2a scenario.

This study also has a few shortcomings and suggests several areas for future work. Firstly, more GCMs with high resolution will be downscaled to evaluate the future temperature and precipitation using more downscaling methods. If possible, the research place should be enlarged to a bigger area because it could be more conducive to the application of a variety of GCMs. In addition, the time scales of simulation, sub-basins discretization, and HRU definition will be improved. For example, a monthly time step will change into a weekly time step and more HRUs will represent the immense topographical and land use variability. Finally, more complicated hydrological cycle will be considered for fully assess water resources, especially in society-relevant extreme events such as sudden floods, rain on snow events, or drought events.

References

Abbaspour KC, Yang J, Maximov I, Siber R, Bogner K, Mieleitner J, Zobrist J, Srinivasan R (2007) Modelling hydrology and water quality in the pre-alpine/alpine thur watershed using SWAT. J Hydrol 333(2):413–430

Arnold JG, Srinivasan R, Muttiah RS, Williams JR (1998) Large area hydrologic modeling and assessment part I: model development 1. JAWRA J Am Water Resour Assoc 34(1):73–89

Babel MS, Bhusal SP, Wahid SM, Agarwal A (2013) Climate change and water resources in the Bagmati river basin Nepal. Theor Appl Climatol 115:639–654

Bader D, Covey C, Gutowski W, Held I, Kunkel K, Miller R, Tokmakian R, Zhang M, (2008) Climate models: an assessment of strengths and limitations. A report by the US Climate Change Science Program and the Subcommittee on Global Change Research, Office of Biological and Environmental Research, Department of Energy, Washington, DC

Buytaert W, Célleri R, Timbe L (2009) Predicting climate change impacts on water resources in the tropical Andes: effects of GCM uncertainty. Geophys Res Lett 36(7):L7406

Chen J, Brissette FP, Leconte R (2011) Uncertainty of downscaling method in quantifying the impact of climate change on hydrology. J Hydrol 401(3):190–202

Chung SW, Gassman PW, Gu R, Kanwar RS (2002) Evaluation of EPIC for assessing tile flow and nitrogen losses for alternative agricultural management systems. Trans Asae 45(4):1135–1146

Coumou D, Rahmstorf S (2012) A decade of weather extremes. Nat Clim Change 2(7):491–496

Dile YT, Berndtsson R, Setegn SG (2013) Hydrological response to climate change for gilgel abay river, in the lake tana basin-upper blue nile basin of Ethiopia. PLoS ONE 8(10):e79296

Duan W, He B, Takara K, Luo P, Hu M, Alias NE, Nover D (2015) Changes of precipitation amounts and extremes over Japan between 1901 and 2012 and their connection to climate indices. Clim Dyn 45(7–8):2273–2292

Fowler HJ, Blenkinsop S, Tebaldi C (2007) Linking climate change modelling to impacts studies: recent advances in downscaling techniques for hydrological modelling. Int J Climatol 27(12):1547–1578

Green CH, Van Griensven A (2008) Autocalibration in hydrologic modeling: using SWAT2005 in small-scale watersheds. Environ Model Softw 23(4):422–434

He B, Takara K, Yamashiki Y, Kobayashi K, Luo P (2011) Statistical analysis of present and future river water temperature in cold regions using downscaled GCMs data. Disaster Prev Res Inst Annu B 54(B):103–111

Khan MS, Coulibaly P, Dibike Y (2006) Uncertainty analysis of statistical downscaling methods. J Hydrol 319(1):357–382

Konikow LF, Kendy E (2005) Groundwater depletion: a global problem. Hydrogeol J 13(1):317–320

Li Z, Zheng F, Liu W, Jiang D (2012) Spatially downscaling GCMs outputs to project changes in extreme precipitation and temperature events on the Loess Plateau of China during the 21st century. Glob Planet Change 82:65–73

Ma X, Yoshikane T, Hara M, Wakazuki Y, Takahashi HG, Kimura F (2010) Hydrological response to future climate change in the Agano river basin, Japan. Hydrol Res Lett 4:25–29

Maurer EP, Duffy PB (2005) Uncertainty in projections of streamflow changes due to climate change in California. Geophys Res Lett 32(3):L3704

Meenu R, Rehana S, Mujumdar PP (2013) Assessment of hydrologic impacts of climate change in Tunga-Bhadra river basin, India with HEC-HMS and SDSM. Hydrol Process 27(11):1572–1589

Narsimlu B, Gosain AK, Chahar BR (2013) Assessment of future climate change impacts on water resources of upper sind river basin, India using SWAT model. Water Resour Manag 27(10):3647–3662

Nash J, Sutcliffe JV (1970) River flow forecasting through conceptual models part I—A discussion of principles. J Hydrol 10(3):282–290

Neitsch SL, Arnold JG, Kiniry JR, Williams JR, King KW (2005) SWAT theoretical documentation version 2005. Blackland Research Center, Temple

Oki T, Kanae S (2006) Global hydrological cycles and world water resources. Science 313(5790):1068–1072

Prudhomme C, Davies H (2009) Assessing uncertainties in climate change impact analyses on the river flow regimes in the UK. Part 1: baseline climate. Clim Change 93(1–2):177–195

Prudhomme C, Reynard N, Crooks S (2002) Downscaling of global climate models for flood frequency analysis: where are we now? Hydrol Process 16(6):1137–1150

Santhi C, Arnold JG, Williams JR, Dugas WA, Srinivasan R, Hauck LM (2001) Validation of the SWAT model on a large river basin with point and non point source. J Am Water Resour Assoc 37(5):1169–1188

Sato Y, Kojiri T, Michihiro Y, Suzuki Y, Nakakita E (2013) Assessment of climate change impacts on river discharge in Japan using the super-high-resolution MRI-AGCM. Hydrol Process 27(23):3264–3279

Setegn SG, Rayner D, Melesse AM, Dargahi B, Srinivasan R (2011) Impact of climate change on the hydroclimatology of lake Tana basin Ethiopia. Water Resour Res 47(4):W4511

Solomon S (2007) Climate change 2007-the physical science basis: working group I contribution to the fourth assessment report of the IPCC. Cambridge University Press, Cambridge, p 1056

Tatsumi K, Oizumi T, Yamashiki Y (2013) Introduction of daily minimum and maximum temperature change signals in the Shikoku region using the statistical downscaling method by GCMs. Hydrol Res Lett 7(3):48–53

Tatsumi K, Oizumi T, Yamashiki Y (2014) Effects of climate change on daily minimum and maximum temperatures and cloudiness in the Shikoku region: a statistical downscaling model approach. Theor Appl Climatol 120(1–2):87–98

Taye MT, Ntegeka V, Ogiramoi NP, Willems P (2011) Assessment of climate change impact on hydrological extremes in two source regions of the Nile river basin. Hydrol Earth Syst Sci 15(1):209–222

Wada Y, van Beek LP, van Kempen CM, Reckman JW, Vasak S, Bierkens MF (2010) Global depletion of groundwater resources. Geophys Res Lett 37(20):L20402

Wilby RL, Dawson CW, (2007) SDSM 4.2-A decision support tool for the assessment of regional climate change impacts, Version 4.2 user manual. Lancaster University, Lancaster/Environment Agency of England and Wales

Wilby RL, Hay LE, Leavesley GH (1999) A comparison of downscaled and raw GCM output: implications for climate change scenarios in the San Juan river basin Colorado. J. Hydrol. 225(1):67–91

Wilby RL, Hay LE, Gutowski WJ, Arritt RW, Takle ES, Pan Z, Leavesley GH, Clark MP (2000) Hydrological responses to dynamically and statistically downscaled climate model output. Geophys Res Lett 27(8):1199–1202

Wilby RL, Dawson CW, Barrow EM (2002) SDSM—a decision support tool for the assessment of regional climate change impacts. Environ Model Softw 17(2):145–157

Zhang X, Zwiers FW, Hegerl GC, Lambert FH, Gillett NP, Solomon S, Stott PA, Nozawa T (2007) Detection of human influence on twentieth-century precipitation trends. Nature 448(7152):461–465